https://doi.org/10.5194/egusphere-2022-361
Preprint. Discussion started: 31 May 2022

Turbulent kinetic energy dissipation rate and associated fluxes in the western tropical Atlantic estimated from ocean glider observations

Peter M.F. Sheehan[1], Gillian M. Damerell[1], Philip J. Leadbitter[1], Karen J. Heywood[1], and Rob A. Hall[1]

[1]Centre for Ocean and Atmospheric Sciences, School of Environmental Science, University of East Anglia, Norwich, NR4 7TJ, United Kingdom

Correspondence: Peter Sheehan (p.sheehan@uea.ac.uk)

Abstract. Ocean gliders enable us to collect the high-resolution microstructure observations necessary to calculate the dissipation rate of turbulent kinetic energy, ε, on timescales of weeks to months: far longer than is normally possible using traditional ship-based platforms. Slocum gliders have previously been used to this end; here, we report the first detailed estimates of ε calculated using the Batchelor spectrum method on observations collected by a FP07 fast thermistor mounted on a Seaglider. We use these same fast thermistor observations to calculate ε following the Thorpe scale method and find very good agreement between the two methods. The Thorpe scale method yields larger values of ε, but the average difference, which is less than an order of magnitude, is smaller than reported elsewhere. The spatio-temporal distribution of ε is comparable for both methods. Maximum values of ε (10^{-7} W kg^{-1}) are observed in the surface mixed layer; values of approximately 10^{-9} W kg^{-} are observed between approximately 200 and 500 m depth. These two layers are separated by a 100 m thick layer of low ε (10^{-10} W kg^{-1}), which is co-located with a high-salinity layer of Subtropical Underwater and a peak in the strength of stratification. We calculate the turbulent heat and salt fluxes associated with the observed turbulence. Between 200 and 500 m, ε induces downward fluxes of both properties that, if typical of the annual average, would have a very small influence on the heat and salt content of the overlying salinity-maximum layer. We compare these turbulent fluxes with estimates of double-diffusive fluxes, having objectively identified those regions of the water column where double diffusion is likely to occur. We find that the double-diffusive fluxes of both heat and salt are larger than the corresponding mechanical fluxes.

1 Introduction

Turbulence in the ocean, and the mixing of different water masses that it induces, are of fundamental importance to ocean dynamics. Over relatively small scales, turbulent mixing often controls the distribution of key water mass properties and tracers; over the world ocean, the sum of these small-scale processes is responsible for the closure of the thermohaline circulation and for the primary production that relies on the upward flux of nutrients to the euphotic zone.

Estimating the dissipation rate of turbulent kinetic energy, ε, by applying the Batchelor spectrum method (Batchelor, 1959) to high-resolution observations of shear and temperature (e.g. Lueck et al., 2002; Peterson and Fer, 2014; Scheifele et al., 2018) has, historically, required considerable ship time, plus specialist instruments and expertise. Consequently, spectrum-based estimates having been difficult to acquire, there are relatively few of them; for instance, Fernández-Castro et al. (2014)

https://doi.org/10.5194/egusphere-2022-361
Preprint. Discussion started: 31 May 2022

collect only 50 profiles of ε from a circumnavigation of the tropics. Methods such as Thorpe scaling (Thorpe, 1977) and fine-scale parameterisation (Polzin et al., 2014; Whalen et al., 2015) have been developed to enable ε to be estimated from ordinary observations of temperature, salinity and velocity. Yet, although non-spectral methods do not require specialist instruments and may be applied to ordinary oceanographic observations (e.g. Fer et al., 2010b; Whalen et al., 2012, 2015), these methods are dependent on more assumptions, and their results tend not to be valid over as wide a range of conditions as those of spectral methods (Polzin et al., 2014; Whalen, 2021). Thus, despite the widespread application of the Thorpe scale and fine-scale parameterisation methods, the potential remains for discrepancies between spectrum- and non-spectrum-based estimates of ε (Howatt et al., 2021).

Given the proliferation in the use of buoyancy-driven ocean gliders over the last decade, there is growing interest in using them to collect the high-resolution microstructure observations necessary to estimate ε using spectral methods. Because of a glider's smooth flight through the water column, it resembles the free-falling, loosely tethered profilers traditionally used to collect microstructure observations. A growing body of literature makes use of microstructure observations collected by gliders, as well as setting out the best ways of processing such data sets (e.g. Fer et al., 2010b; Peterson and Fer, 2014; Palmer et al., 2015; Schultze et al., 2017; Scheifele et al., 2018; Scott et al., 2021). Up until now, the vast majority of studies, and in particular those studies that estimate ε using spectral methods, have used shear observations collected by Slocum gliders (Palmer et al., 2015); observational studies of turbulence using other autonomous platforms are known to be lacking (Frajka-Williams et al., 2021). Some authors have also used fast thermistor data to estimate ε (Scheifele et al., 2018), while Rainville et al. (2017) briefly discuss the microstructure system developed for use on Seagliders, another commonly used glider platform, and present spectrum-based estimates of the rate of destruction of temperature-gradient variance, χ. Here, we report in detail the first spectrum-based estimates of ε calculated from fast thermistor Seaglider observations, and we compare the results with estimates of ε calculated by applying the Thorpe scale method to the same observations.

The western tropical Atlantic (Fig. 1) is known for the persistent presence of the salt fingering regime of double-diffusion (Schmitt et al., 1987; Rollo et al., 2022). For salt fingering to occur, warm, saline water must overlie cooler, fresher water: the water column is therefore stably stratified by temperature but unstably stratified by salinity. Such conditions are maintained in the western tropical Atlantic by the presence of Subtropical Underwater (SUW) at the base of the mixed layer, a warm, high-salinity water mass common to tropical regions (Schmitt et al., 1987; Fer et al., 2010a). Beneath SUW, temperature and salinity both decrease with depth. In a salt fingering regime, the slow molecular diffusion of salt relative to the fast diffusion of heat leads to the development of salt fingers: narrow, small-scale filaments of alternately upwelling warming water and downwelling cooling water. Over time, double-diffusive convection and salt fingers promote the formation of thermohaline staircases: temperature and salinity profiles characterised by a series of homogeneous mixed layers separated by sharp, narrow gradient layers. Such staircases have previously been observed in the western tropical Atlantic (Schmitt et al., 1987; Rollo et al., 2022). Importantly for studies of ocean mixing, double diffusive convection enables the vertical transport of heat and salt by a mechanism other than the mechanical, turbulent mixing captured by ε.

Here, we use high-resolution temperature microstructure observations collected by a Seaglider to estimate ε using the Batchelor spectrum method (Sec. 2.2; Batchelor, 1959) and using the Thorpe scale method (Sec. 2.3; Thorpe, 1977), and compare the

https://doi.org/10.5194/egusphere-2022-361
Preprint. Discussion started: 31 May 2022

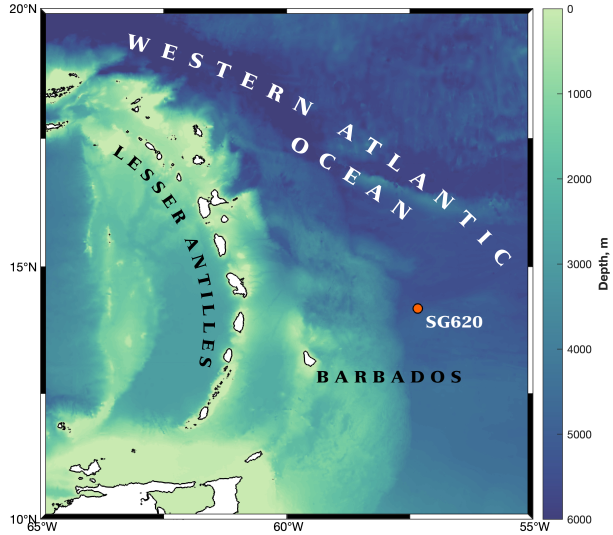

Figure 1. Bathymetry (m) of the western tropical Atlantic and the the eastern Caribbean Sea in the region of the Lesser Antilles. The location of SG620, northeast of Barbados, is marked by the orange circle. Bathymetric data are extracted from the GEBCO 2020 grid (www.gebco.net)

results (Sec. 3.1). From these estimates of ε, we derive turbulent fluxes of heat and salt through an observed layer of elevated ε, (Sec. 3.2), and compare these with heat and salt fluxes driven by double-diffusive mixing (Sec. 3.3). We discuss the results in Sec. 4.

2 Data and methods

2.1 Glider observations

As part of the EUREC4A field campaign (Stevens et al., 2021), Seaglider 620 was deployed at 14.2°N, 57.3°W, approximately 200 km northeast of Barbados (Fig. 1) on 23 January 2020. It completed 131 dives to 750 m before being recovered on 5 February 2020. The glider carried an unpumped CT sail measuring in situ conductivity and temperature, and a microstructure system. Given the shape of the Seaglider's hull, it is not possible to mount an all-in-one microstructure payload, such as the RSI MicroRider that is used on Slocum gliders (e.g., Fer et al., 2014; Schultze et al., 2017; Scheifele et al., 2018). Instead, a reconfigured payload is used, one consisting of a pair of RSI MicroPod sensor modules mounted either side of the CT sail, and a dedicated pressure housing containing the system's DataLogger mounted inside the Seaglider's aft fairing (Creed et al., 2015). The system draws its power from the Seaglider and was developed and manufactured by Rockland Scientific International.

During the EUREC4A campaign, the glider was equipped with one MicroPod carrying a shear probe and one MicroPod carrying an FP07 fast-response temperature probe. The FP07 probe samples at 512 Hz and has a sensitivity of better than 0.1 mK (Sommer et al., 2013). Microstructure temperature observations are better suited than shear observations to estimating

https://doi.org/10.5194/egusphere-2022-361
Preprint. Discussion started: 31 May 2022

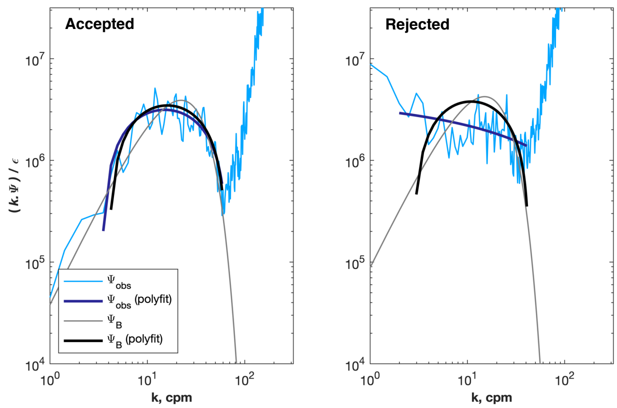

Figure 2. Example of temperature spectra, Ψ, that were accepted (left) and rejected (right) by the quality control algorithm. Observed and theoretical spectra are shown by the thin, light-coloured lines; the second-order polynomial fits are shown by thick, dark-coloured lines.

ε in low-dissipation environments (Scheifele et al., 2018), and have the added advantage of being less readily contaminated by platform vibration (Frajka-Williams et al., 2021); here we focus on the temperature-based estimates of epsilon. The glider's hydrodynamic flight model, which is used to estimate along-path speed, is tuned following Frajka-Williams et al. (2011), and the thermal lag of the standard CT sail is corrected following Garau et al. (2011).

2.2 Estimating ε using spectral methods

We estimate ε from the glider's fast thermistor temperature observations using the Batchelor spectrum method; we hereafter refer to these estimates as ε_μ. For this, we use the Matlab toolbox produced by Benjamin Scheifele and Jeffrey Carpenter (github.com/bscheife/turbulence_temperature) and recently used by Howatt et al. (2021). The method is described in detail by Scheifele et al. (2018), and much of the underlying theory, and a similar methodology, are described by Peterson and Fer (2014), so we here give only an outline.

We divide the temperature time series from the FP07 thermistor into half-overlapping segments of 32 seconds length. Within each 32-second segment, we further divide the measurements into 15 four-second, half-overlapping sub-segments. From each sub-segment, we calculate a temperature power spectrum, Δ_4. We then average these 15 Δ_4 to produce one power spectrum, Δ_{32}, that is representative of the original 32-second segment. We convert each Δ_{32} from frequency space to wavenumber space (Fig. 2) using the glider's along-path speed averaged over the same 32 seconds, and assuming the validity of Taylor's frozen turbulence hypothesis (Scheifele et al., 2018).

We transform each Δ_{32} into a temperature-gradient spectrum, Ψ, which should resemble the Batchelor spectrum, Ψ_B (Batchelor, 1959), the theoretical spectrum that describes temperature-gradient spectra and which is commonly used when calculating ε_μ (e.g. Peterson and Fer, 2014; Scheifele et al., 2018). The Batchelor spectrum is a function of k_B, the Batchelor wavenumber, and of χ, the rate of destruction of temperature-gradient variance (Osborn and Cox, 1972). A comprehensive mathematical

https://doi.org/10.5194/egusphere-2022-361
Preprint. Discussion started: 31 May 2022

treatment of the use of Ψ_B when estimating ε is given by Peterson and Fer (2014). Here, we require k_B in order to calculate ε_μ (W kg^{-1}) according to:

$$\varepsilon_\mu = \nu D_T^2 (2\pi k_B)^4 \tag{1}$$

where ν is the kinematic viscosity of seawater, $D_T = 1.44 \times 10^{-7}$ m^2 s^{-1} is the molecular diffusion coefficient of temperature.

We calculate χ according to:

$$\begin{aligned} \chi &= \chi_l + \chi_{obs} + \chi_u \\ &= 6D_T \left(\int_0^{k_l} \Psi_B \, dk + \int_{k_l}^{k_u} \Psi \, dk + \int_{k_u}^{\infty} \Psi_B \, dk \right) \end{aligned} \tag{2}$$

where χ_{obs} is that part of χ derived by integrating Ψ, and χ_l and χ_u are correction terms derived from Ψ_B. The factor of six comes from assuming isotropic turbulence. The wavenumbers k_l and k_u are, respectively, the lower and upper wavenumber limits of the range over which Ψ is considered reliable; the criteria for choosing k_l and k_u are explained fully by Scheifele et al. (2018). Given an estimate of χ, the maximum likelihood estimation procedure of Ruddick et al. (2000) is used to find the value of k_B where Ψ_B is the best fit to Ψ between k_l and k_u. On the first iteration, χ_l and χ_u are set to zero and hence $\chi = \chi_{obs}$. On subsequent iterations, the previous value of χ and the previous best-fit value of k_B are used to estimate Ψ_B and hence χ_l and χ_u, and the estimate of k_B is further refined.

An observed spectrum that deviates from the shape of the relevant theoretical spectrum should not be used to estimate ε_μ. To discriminate between acceptably and unacceptably shaped spectra, we fit second order polynomials of the form:

$$P(k) = a.log_{10}(k)^2 + b.log_{10}(k) + c \tag{3}$$

to both the observed and the theoretical spectra, following the method of Scott et al. (2021), where k is wavenumber and a, b and c are the polynomial coefficients to be determined. Prior to fitting, we normalise each spectrum by dividing by its corresponding estimate of ε_μ; this enables the same criteria to be used when assessing goodness-of-fit over spectra that otherwise span many orders of magnitude. We also multiply spectra by k in order to preserve variance. P is defined over the same range of wavenumbers over which the observed spectrum is integrated when estimating χ.

We accept a spectrum if:

1. The value of a fitted to Ψ is positive. (Note that a fitted to Ψ_B is always positive.)

2. The ratio of the a values fitted to Ψ_B and Ψ (a_{Ψ_B}/a_Ψ) is less than two.

In addition, following Scheifele et al. (2018), we remove an estimate of ε_μ if:

https://doi.org/10.5194/egusphere-2022-361
Preprint. Discussion started: 31 May 2022

3. Fewer than six points are included in the spectra fit.

4. If the quantity $U/(\varepsilon_\mu/N)^{1/2}$ is less than five, where U is the glider's speed-in-direction-or-travel, indicating that Tayor's frozen turbulence hypothesis is invalid.

5. If the sum of the correction terms χ_u and χ_l is greater than the observed term χ_{obs} (Eqn 2).

Finally, following Peterson and Fer (2014), we remove an estimate of ε_μ if:

6. The mean absolute deviation, which quantifies the goodness of fit between Ψ_{obs} and Ψ_B, is greater than $2(2/d)^{1/2}$, where d is the degrees of freedom, calculated as 1.9 multiplied by the number of sub-segments within each 32-second segment, i.e., 1.9×15.

Examples of accepted and rejected spectra are presented in Fig. 2. After quality control, 84% of ε_μ estimates remained. Quality-controlled estimates of ε_μ were binned, profile by profile, into 25 m bins; we use the geometric mean (and standard deviation) in preference to the arithmetic mean, the better to represent the average (and spread) of observations that span many orders of magnitude.

2.3 Thorpe scale estimates

We apply the Thorpe scale method (Thorpe, 1977) to the FP07 temperature measurements to derive a second, independent estimate of the turbulent kinetic energy dissipation rate, hereafter referred to as ε_T. The sampling frequency of the FP07 thermistor (512 Hz) is faster than its true response time, which Sommer et al. (2013) estimate to be 10 ms (i.e. 100 Hz). Consequently, we apply a low-pass, 12th-order Butterworth filter with a cut-off frequency of 100 Hz to remove the highest-frequency variability. This prevents instrumental noise erroneously manifesting as small density overturns (Mater et al., 2015; Ijichi and Hibiya, 2018). Temperature observations were then binned (mean-averaged) into 10 ms bins, giving an effective vertical resolution of 3 ± 0.5 mm.

Each temperature profile is then re-ordered in depth so that it is stable in temperature. From the re-ordered profile we calculate the vertical Thorpe displacement, Δz: the difference between an observation's original depth and its re-ordered depth. We identify an overturn as a vertical segment in which the cumulative sum of Δz is non-zero, and which is bounded above and below by segments in which the cumulative sum of Δz is zero. Following Ijichi and Hibiya (2018), we combine all overturns that are smaller than 2 m and are within 1 m of an adjacent overturn until the region is larger than 2 m. The Thorpe scale, L_T (m), is then the root mean square of Δz over an overturn:

$$L_T = \langle \Delta z^2 \rangle^{1/2} \tag{4}$$

https://doi.org/10.5194/egusphere-2022-361
Preprint. Discussion started: 31 May 2022

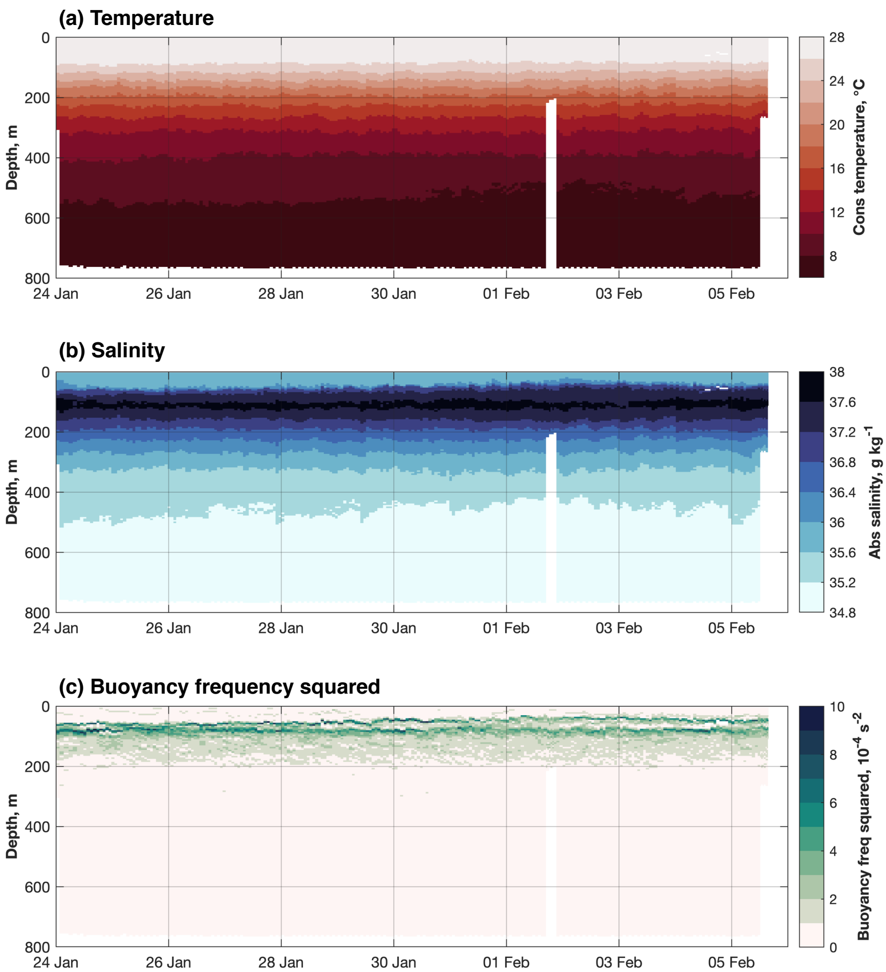

Figure 3. Time series of hydrographic observations from SG620, averaged into 5 m bins: **(a)** conservative temperature (°C), **(b)** absolute salinity (g kg^{-1}), and **(c)** buoyancy frequency squared (N^2; s^{-2}).

where angular brackets indicate the mean. Finally, we calculate ε_T (W kg^{-1}) from L_T by relating the Ozmidov scale, $L_O = (\varepsilon_T/N^3)^{1/2}$ (Ozmidov, 1965), to the Thorpe scale by the empirical relation $L_O = 0.8\ L_T$ (Dillon, 1982), which yields:

$$\varepsilon_T = 0.64 L_T^2 N^3 \tag{5}$$

where N is the buoyancy frequency calculated using temperature and salinity observations from the glider's CT sail (binned at 5 m resolution).

We visually inspect estimates of ε_T and remove unphysical results: for example regions that exhibit very clear distinctions compared with the surrounding water column, typically characterised by highly elevated values of ε_T. Estimates of ε_T were

https://doi.org/10.5194/egusphere-2022-361
Preprint. Discussion started: 31 May 2022

binned into 25 m bins using the geometric mean. Temperature is a poor proxy for density in any region of the water column where salinity is the dominant control on density; consequently, regions of the water column with large salinity variability but little temperature variability can falsely appear to be overturns, or can appear to not contain overturns which are present in reality. To identify such regions, we calculate, within each 25 m bin, the ratio, r between the standard deviation of absolute salinity, S, and conservative temperature, Θ:

$$r = \frac{std.dev(S)}{std.dev(\Theta)} \tag{6}$$

Values of r are then normalised: we subtract the mean of r (calculated over the entire data set) and divide by its standard deviation. The mean and standard deviation of $log(r)$ are calculated to limit the influence of bins with extreme values of r. We remove values of ε_T from bins with a normalised r that is greater than or equal to a critical value of 0.5. A range of critical values was investigated; a critical value of 0.5 provided the best compromise between algorithmically removing high values and removing too many data points.

3 Results

3.1 Estimates of ε

The water masses observed are typical of the region (e.g. Schmitt et al., 1987). A warm (> 26 °C) surface mixed layer of intermediate salinity overlies SUW, a salinity-maximum (> 37.6 g kg^{-1}) layer located in the upper thermocline (Fig. 3). Beneath SUW, temperature and salinity steadily decrease with depth into the Antarctic Intermediate Water layer that lies beneath (Fig. 3). Two maxima in buoyancy frequency are observed: an upper maximum at the base of the surface isohaline layer, and a lower maximum at the base of the surface isothermal layer (Fig. 3).

There is generally good agreement between ε_μ and ε_T (Figs. 4 and 5). The higher of the two is ε_T, as can be seen in the depth-time distributions and mean profiles (Fig. 4), and in the histograms (Fig. 5). The spatio-temporal geometric mean of ε_μ is 3.52 × 10^{-10} W kg^{-1}; the spatio-temporal geometric mean of ε_T is 4.96 × 10^{-10} W kg^{-1}. (Each mean is calculated only from grid boxes with estimates from both methods.) The distribution of ε_T is the noisier of the two and contains higher values at depth: values of ε_μ greater than 10^{-7} W kg^{-1} are not observed below 100 m (Fig. 4), whereas values of ε_T greater than 10^{-7} W kg^{-1} are on occasion observed below 100 m (Fig. 4). The greater noise in ε_T is reflected in its having a higher standard deviation (5.57) than ε_μ (3.94). (Note that geometric standard deviation is multiplicative, not additive.)

The highest values of ε are found in approximately the top 100 m of the water column (Fig. 4; ε_μ only), in the surface mixed layer (Fig. 3), where ε values in excess of 10^{-7} W kg^{-1} are frequently observed. Values of ε_μ as low as 10^{-11} W kg^{-1} are also observed in the surface mixed layer, albeit less frequently. Hence, the mean ε_μ in the upper water column (< 10^{-9} W kg^{-1}) is larger than at other depths, but the standard deviation (approximately 10^{-2} W kg^{-1}) is also larger than at other depths (Fig. 4; right-hand panels).

https://doi.org/10.5194/egusphere-2022-361
Preprint. Discussion started: 31 May 2022

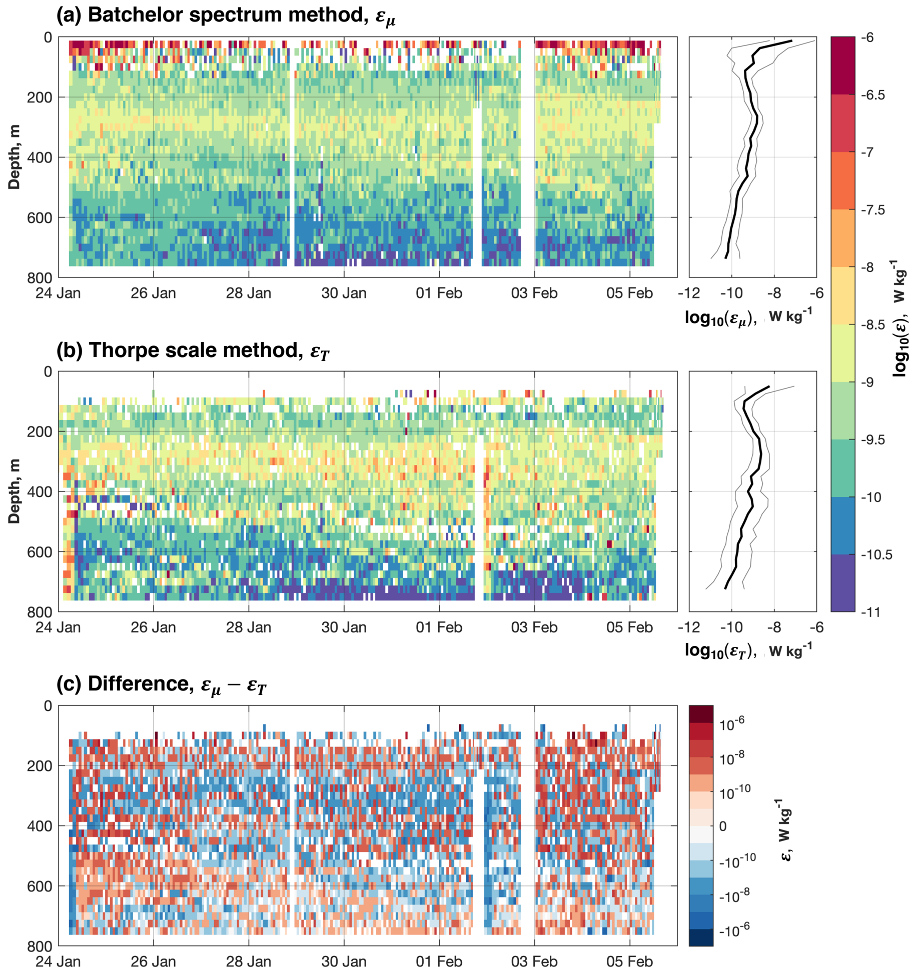

Figure 4. Turbulent kinetic energy dissipation rate, ε (W kg^{-1}) as estimated using **(a)** the Batchelor spectrum method (ε_μ) and **(b)** the Thorpe scale method (ε_T). The respective means (thick line) and standard deviations (thin lines) are shown in the panels on the right. Note that geometric standard deviation is multiplicative. **(c)** The difference between ε_μ and ε_T.

Immediately below the high-ε surface mixed layer, a thin layer of relatively low ε lies within SUW in the upper thermocline, between approximately 100 and 200 m (Figs. 3 and 4). Here, values of both ε_μ and ε_T are commonly between $10^{-9.5}$ and 10^{-9} W kg^{-1}. This low-ε layer is clearly seen in the mean profiles (Fig. 4). Below the upper boundary of SUW, found between at 50 to 75 m, highest values of ε are less frequently observed (Figs. 4 and 3). The upper boundary corresponds to the shallowest band of high buoyancy frequency (Fig. 3); a peak in the strength of the stratification that might be expected to arrest the downward penetration of surface mixing.

Below this low-ε SUW layer, between approximately 200 and 500 m, is a relatively thick layer with higher values of ε ($10^{-9} < \varepsilon < 10^{-8}$ W kg^{-1}; Fig. 4). Values of ε_T in this layer are generally higher than values of ε_μ (Fig. 4), which would

https://doi.org/10.5194/egusphere-2022-361
Preprint. Discussion started: 31 May 2022

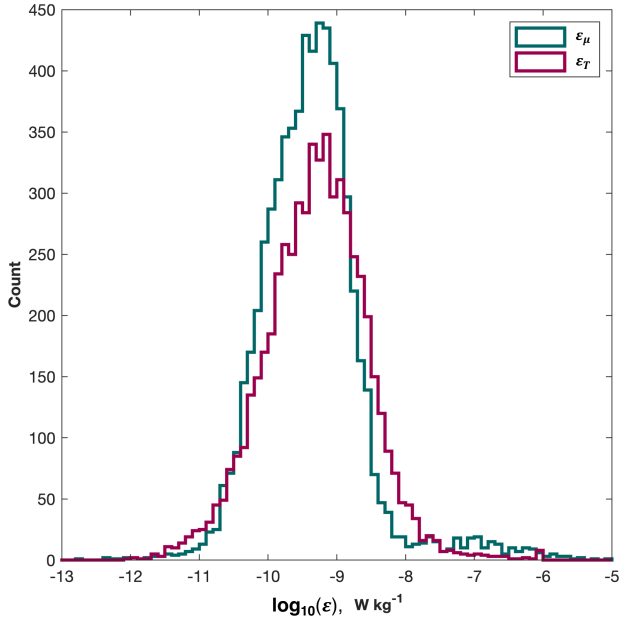

Figure 5. Histograms of turbulent kinetic energy dissipation rate as estimated using the Batchelor spectrum method (green line) and the Thorpe scale method (purple line; both W kg^{-1}).

explain why the distribution of ε_μ is slightly skewed to lower values, while the distribution of ε_T is slightly skewed to higher values (Fig. 5a). A few values of ε_T are in excess of $10^{-7.5}$ W kg^{-1} (Fig. 4). These high values are typically those in the modest secondary peak in the distribution of ε_T between 10^{-6} and 10^{-5} W kg^{-1} (Fig. 5). The thickness of this higher-ε_μ and -ε_T layer increases by 50 to 100 m over the course of the deployment. Below 700 m, both ε_μ and ε_T are less than 10^{-10} W kg^{-1} between 28 January and 4 February; the differences between the two estimates also tend to be lower within this spatio-temporal range (Fig. 4c). This is in contrast to higher values of ε_μ and $\varepsilon_T (< 10^{-11}$ W kg^{-1}) within the 700 to 800 m depth range at the beginning and end of the deployment.

3.2 Heat and salt fluxes

We use the Osborn relation to calculate diapycnal diffusivity, κ_ρ (m^2 s^{-1}):

$$\kappa_\rho = \Gamma \frac{\varepsilon}{N^2} \tag{7}$$

where Γ is mixing efficiency, which is here taken to be 0.2 (Osborn, 1980). We use ε_μ in preference to ε_T because ε_μ has better coverage in the mixed layer (Fig. 4).

https://doi.org/10.5194/egusphere-2022-361
Preprint. Discussion started: 31 May 2022

The distribution of κ_ρ resembles that of ε_μ, notwithstanding a decrease in κ_ρ at mid-depth between the 26 and 28 January where ε_μ remains relatively high (Figs. 4a and 6a). Excluding the surface mixed layer, κ_ρ is highest between 400 and 500 m (< $10^{-4.5}$ m^2 s^{-1}; Fig. 6a), with low values predominating in the core of the high-salinity SUW (< 10^{-6} m^2 s^{-1}; Fig. 6a).

Vertical turbulent heat and salt fluxes, Q_h (W m^{-2}) and Q_S (kg m^{-2} s^{-1}) respectively, can be calculated from κ_ρ:

$$Q_h = -\rho C_p \kappa_\rho \Theta_z \tag{8}$$

$$Q_S = \frac{1}{1000}(-\rho \kappa_\rho S_z) \tag{9}$$

where ρ is density, C_p is the specific heat capacity of seawater, Θ_z is the vertical gradient of conservative temperature, and S_z is the vertical gradient of absolute salinity.

Beneath the surface mixed layer, both Q_h and Q_S are predominantly negative (i.e. downward) because temperature and salinity decrease with depth (Fig. 3a and b). The most prominent feature of the distributions of both is the broad region of negative (i.e. downward) turbulent heat and salt transport between approximately 200 and 500 m (Fig. 6b and c). This corresponds to the elevated values of ε ($> 10^{-5}$) found within same depth range (Fig. 6a). Within the surface mixed layer, notwithstanding the limited coverage of the observations, Q_h is positive in the top 50 m and negative between 50 and 100 m; by contrast, Q_S is positive throughout the surface mixed layer (Fig. 6b and c).

Over the period of the observations, the mean Q_h between 200 and 500 m was -1.45 W m^{-2}; integrated over a year, this results in an annual turbulent heat flux of -4.58×10^7 J m^{-2}. Over the period of the observations, the mean Q_S between 200 and 500 m was -6.03×10^{-8} kg m^{-2} s^{-1}; integrated over a year, this results in an annual turbulent salt flux of -1.90 kg m^{-2}.

These fluxes, being derived from ε, represent transports of heat and salt that are driven by turbulent, mechanical mixing. This is a relatively low-turbulence region, and the fluxes are correspondingly relatively small. For instance, we estimate that the annually integrated turbulent fluxes would reduce the temperature and salinity of the overlying SUW layer (assumed to be 100 m thick) by 0.11°C and 0.02 g kg^{-1} respectively. However, these estimates do not account for the fluxes driven by the double-diffusive mixing characteristic of the thermohaline staircases that are prominent in the western tropical Atlantic (Schmitt et al., 1987; Rollo et al., 2022); Seaglider 620 was deployed at the edge of the region identified by Schmitt et al. (1987) as being the location of strong staircase structures. In low-turbulence regimes, double-diffusive mixing gives rise to fluxes that can be larger than those driven by mechanical turbulence (Schmitt, 1988).

3.3 Double diffusion and associated fluxes

We use the algorithm of Rollo et al. (2022) to identify gradient layers in thermohaline staircases: that is, regions of likely active salt fingering in which double diffusive convection occurs. The algorithm identifies both mixed-layers and the gradient-layers between them at 1 m resolution.

https://doi.org/10.5194/egusphere-2022-361
Preprint. Discussion started: 31 May 2022

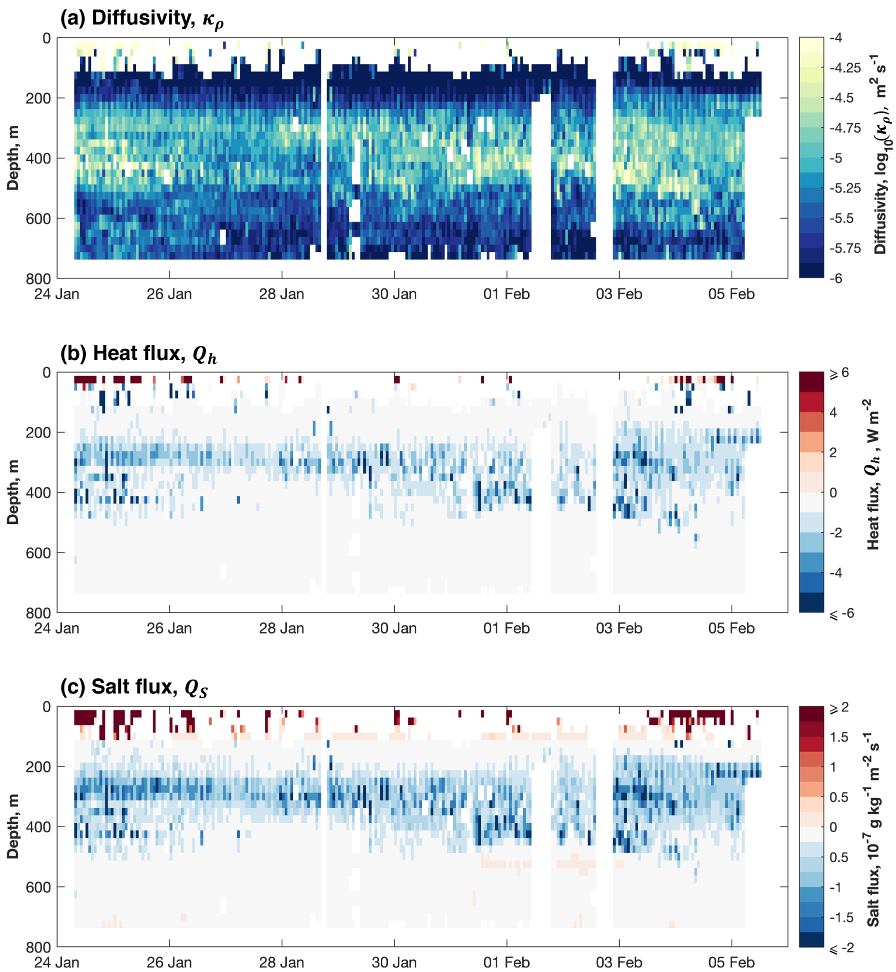

Figure 6. **(a)** Diffusivity, $log_{10}(\kappa_\rho)$ (m^2 s^{-1}). **(b)** Vertical heat flux, Q_h (W m^{-2}). **(c)** Vertical salt flux, Q_S (10^{-7} g kg^{-1} m^{-2} s^{-1}). Negative fluxes are downward. All are calculated from ε calculated using the Batchelor spectrum method.

To estimate haline diffusivity, κ_S, in the presence of salt fingering, and given that theoretical flux laws can overestimate κ_S in the real ocean, we follow van der Boog et al. (2021) in using the empirically determined relations of Radko and Smith (2012):

$$\kappa_S = \left(\frac{135}{(R_\rho - 1)^{1/2}} - 62.75\right) K R_\rho \tag{10}$$

https://doi.org/10.5194/egusphere-2022-361
Preprint. Discussion started: 31 May 2022

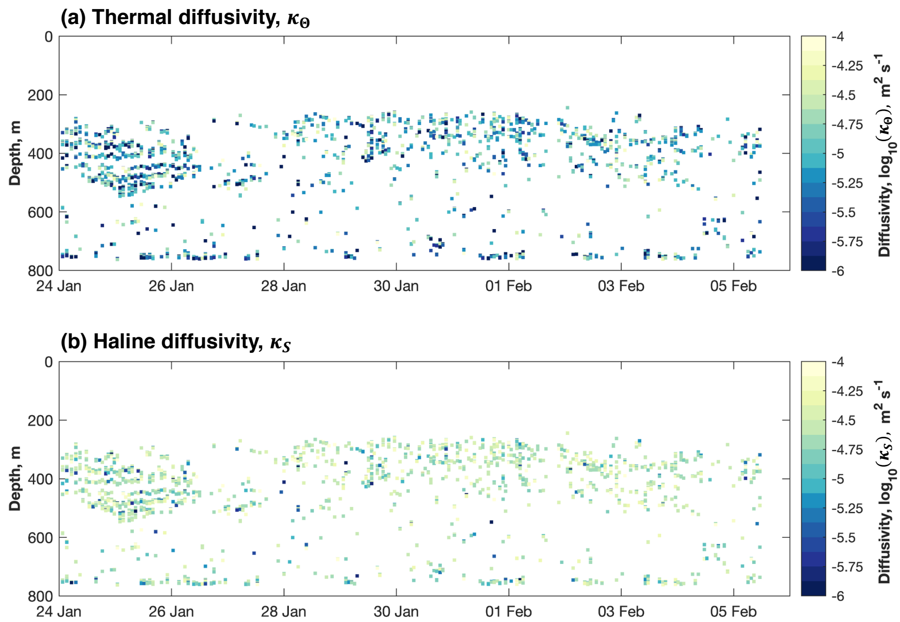

Figure 7. (a) Thermal diffusivity, κ_Θ and **(b)** haline diffusivity, κ_S (both m^2 s^{-1}), in the presence of double-diffusive convection. Both diffusivities are plotted only in gradient layers of thermohaline staircases.

where $R_\rho = \alpha\Theta_z/\beta S_z$ is the density ratio, α is the thermal expansion co-efficient, β is the haline contraction coefficient, and K is the molecular diffusivity of heat. From κ_S, also following van der Boog et al. (2021) and Radko and Smith (2012), we then calculate κ_Θ:

$$\kappa_\Theta = \kappa_S \frac{\gamma}{R_\rho} \tag{11}$$

where $\gamma = 2.709e^{-2.513R_\rho} + 0.5128$ is the density flux ratio in the presence of salt fingers.

Thermal diffusivity in the presence of double diffusion is similar to that caused by mechanical turbulence (Figs. 6a and 7a); haline diffusivity is higher (Figs. 6a and 7b). The mean of κ_ρ between 200 and 500 m is 1.13×10^{-5} m^2 s^{-1}, the mean of κ_Θ is 1.44×10^{-5} m^2 s^{-1}, and the mean of κ_S is 3.12×10^{-5} m^2 s^{-1}. Of course, double-diffusion is spatially and temporally much more patchy, than turbulent mixing, which is spatially and temporally continuous; hence, the mean values of κ_Θ and κ_S are calculated over a much smaller sample region.

Over the period of the observations, the mean double-diffusive heat flux between 200 and 500 m was -5.45 W m^{-2}; integrated over a year, this results in an annual double-diffusive temperature flux of -1.72×10^8 J m^{-2}. Over the period of the observations, the mean double-diffusive salt flux between 200 and 500 m was -5.18×10^{-7} kg m^{-2} s^{-1}; integrated over a year, this results in an annual double-diffusive salt flux of -16.34 kg m^{-2}. Respectively, we estimate that these annually

https://doi.org/10.5194/egusphere-2022-361
Preprint. Discussion started: 31 May 2022

integrated double-diffusive fluxes would reduce the temperature and salinity of the overlying SUW layer (again assumed to be 100 m thick) by 0.42°C and 0.15 g kg^{-1} respectively.

4 Discussion

Our finding that estimates of ε_T are higher than estimates of ε_μ is in agreement with the findings of Howatt et al. (2021). They conclude that, while the Thorpe scale method can well represent the spatio-temporal distribution of ε, shortcomings in CTD sampling and the necessary setting of a minimum Thorpe scale, L_T (Eqn. 4), artificially inflate ε_T by an order of magnitude. The differences between ε_μ and ε_T reported here are not as extreme, being, on average, less than an order of magnitude (Sec. 3; Figs. 4 and 5). The very high resolution of the FP07 thermistor temperature observations (512 Hz; approximately 100 Hz when accounting for the sensor's response time; Sec. 2) should reduce the minimum L_T compared with calculations using observations from a standard glider CT sail; however, the lack of similarly high-resolution salinity observations means that the resolution of N used to calculate ε_T in Eqn. 5 will limit any improvement that a small minimum L_T might otherwise have on estimate of ε_T. Nevertheless, we estimate that the minimum L_T in the present study is 1 m; Howatt et al. (2021), who reduce the difference between their two estimates of ε, report that their minimum L_T is 2 m, so the better agreement between ε_μ and ε_T reported here may be explained by our higher vertical resolution. A further limitation on using the Thorpe scale method to estimate ε from temperature observations alone is that any influence of salinity of density is neglected; we must assume here that density is dominated by temperature. This is a fair assumption in the tropics, especially given that, over much of the upper-ocean in this region, salinity decreases with depth and thus does not dominate density. However, in regions such as the poles where salinity frequently dominates density, the Thorpe scale method applied to temperature observations along would likely not yield reliable results.

Values of ε in the western tropical Atlantic are broadly consistent with other open-ocean regions away from shallow topography. For instance, Sheen et al. (2013) and Naveira Garabato et al. (2016) report background ε values of approximately 10^{-10} to 10^{-9} W kg^{-1} downstream of the Drake Passage, with values in excess of 10^{-8} W kg^{-1} in the upper 1000 m and in the vicinity of rough topography. George et al. (2021) report ε values between 10^{-10} to 10^{-8} W kg^{-1} in the upper layers of the southwestern Bay of Bengal. And Peterson and Fer (2014) report mission-mean values of between 10^{-8} to 10^{-7} W kg^{-1} from observations collected near the Faroe Islands in the northern Atlantic.

Limited estimates of ε are available for the western tropical Atlantic. Two profiles from the region, collected by a microstructure turbulence profiler, were presented by Fernández-Castro et al. (2014). Similarly to our profiles, they find surface ε values between approximately 10^{-7} and 10^{-6} W kg^{-1}, and values between approximately 10^{-9} and 10^{-8} W kg^{-1} between 50 and 300 m. Below 50 m, their estimates of κ_ρ are similar to ours, although they report near-surface values several orders of magnitude larger than ours (e.g. $> 10^{-3}$ m^2 s^{-1}). Two sets of observations taken several years apart and separated by up to hundreds of kilometres cannot be readily compared; moreover, their profiles do not extend deeper than 300 m. Interannual variability and geographic differences could be pronounced. Nevertheless, there is no evidence in their deepest observations of an increase

https://doi.org/10.5194/egusphere-2022-361
Preprint. Discussion started: 31 May 2022

in ε that might indicate the presence of the elevated-ε layer that we observe beneath SUW (Figs. 3 and 4) and which, to our knowledge, has not previously been described.

The dissipation rates presented above appear to have a limited influence on the hydrography of the study region. If the dissipation estimates and resultant fluxes reported above are representative of annual average conditions, heat and salt from the SUW later might be expected to penetrate downwards into the ocean interior relatively slowly. Consequently, the temperature and salinity of SUW would be little changed by downward turbulent mixing. The downward flux of heat due to double diffusion is almost four times that due to turbulent mixing; the downward flux of salt due to double diffusion is 7.5 times that due to turbulent mixing. Nevertheless, integrated over a year, these fluxes are still relatively small. The properties of SUW are likely little influenced by the downward mixing of heat and salt into the ocean interior.

5 Conclusions

We estimate the dissipation rate of turbulent kinetic energy, ε, from high-resolution fast thermistor temperature observations using the Batchelor spectrum-fitting method (ε_μ) and the Thorpe scale method (ε_T). The results from the two methods agree well, although ε_T is on average higher than ε_μ. This is in agreement with previous studies, although the difference reported here, which is less than an order of magnitude, is below that reported elsewhere. We posit that this improved agreement is due to ε_T being calculated using the same high-resolution observations as were used to calculate ε_μ: other studies have compared ε_μ to ε_T calculated using lower-resolution temperature observations. Of the two estimates, ε_T is the noisier.

We identify a layer of elevated ε values between 200 and 500 m that lies immediately below Subtropical Underwater, a high-salinity sub-surface water mass that is co-located with a maximum in stratification. We estimate that, over the period of the deployment, this elevated ε layer is responsible for a mean heat flux of -1.45 W m^{-2} and a mean salt flux of -6.03×10^{-8} kg m^{-2} s^{-1}. Given the prevalence of double diffusion and thermohaline staircases in the region, we estimate a mean double-diffusive heat flux of -5.45 W m^{-2} and a mean double-diffusive salt flux of -5.18×10^{-7} kg m^{-2} s^{-1}. Consequently, both heat and salt fluxes appear to be driven primarily by double diffusion.

Code availability. The Matlab toolbox of Scheifele et al. (2018) to calculate turbulent kinetic energy dissipation rate following the Batchelor spectrum method is available at: github.com/bscheife/turbulence_temperature. The thermohaline staircase detection algorithm of Rollo et al. (2022) is available at: github.com/callumrollo/thermohaline-steps.

Data availability. Standard hydrographic observations from SG620 are available from the British Oceanographic Data Centre at: doi:10/gnz8. Processed turbulent kinetic energy dissipation rate estimates, from both Batchelor and Thorpe scale methods, are available from the British Oceanographic Data Centre at: doi:10/htsw.

https://doi.org/10.5194/egusphere-2022-361
Preprint. Discussion started: 31 May 2022

Author contributions. PMFS and GMD calculated turbulent kinetic energy dissipation rate following the Batchelor spectrum method. PJL calculated turbulent kinetic energy dissipation rate following the Thorpe scale method. All authors contributed to the analysis. PMFS wrote the paper with assistance from GMD and PJL, and with comments and feedback from KJH and RAH.

Competing interests. The authors declare that they have no competing interests.

Acknowledgements. PMFS, GMD, KJH and RAH were supported by the COMPASS project (grant number 741120), which was funded by the European Research Council under the Horizon 2020 programme. PJL was funded by NERC-UKRI NEXUSS PhD studentship NE/N012070/1. We thank Beth Siddle, Callum Rollo, and the crew and scientists of the RV Meteor (cruise M161) for assistance in the deployment and recovery of the glider. We thank Gareth Lee and Marcos Cobas-Garcia for the preparation of the glider, and the UEA glider group for piloting. We thank Callum Rollo for kindly assisting with data processing for the thermohaline staircase detection.

https://doi.org/10.5194/egusphere-2022-361
Preprint. Discussion started: 31 May 2022

References

Batchelor, G. K.: Small-scale variation of convective quantities like temperature in a turbulence fluid. Part one: general discussion and the case of small conductivity, Journal of Fluid Mechanics, 5, 113 133, 1959.

Creed, E., Ross, W., Lueck, R., Stern, P., Douglas, W., Wolk, F., and Hall: Integration of an RSI microstructure sensing package into a Seaglider, Oceans 2015 – MTS/IEEE Washington, 2015.

Dillon, T. M.: Vertical overturns: A comparison of Thorpe and Ozmidov scales, Journal of Geophysical Research, 87, 9601 – 9631, 1982.

Fer, I., Nandi, P., Holbrook, W. S., Schmitt, R. W., and Páramo, P.: Seismic imaging of a thermohaline staircase in the western tropical North Atlantic, Ocean Science, 6, 621 – 631, 2010a.

Fer, I., Skogseth, R., and Geyer, F.: Internal waves and mixing in the marginal ice zone near the Yermak Platuea, Journal of Physical Oceanography, 40, 1613 – 1630, 2010b.

Fer, I., Peterson, A. K., and Ullgren, J. E.: Microstructure measurements from an underwater glider in the turbulent Fareo Bank Channel overflow, Journal of Atmospheric and Oceanic Technology, 31, 1128 – 1150, 2014.

Fernández-Castro, B., Mouriño-Carballido, B., Benítez-Barrios, V. M., Chouciño, P., Fraile-Nuez, E., Graña, R., Piedeleu, M., and Rodríguez-Santana, A.: Micostructure turbulence and diffusivity parameterisation in the tropical and subtropical Atlantic, Pacific and Indian Oceans during the Malaspina 2010 expedition, Deep-Sea Research I, 94, 15 – 30, 2014.

Frajka-Williams, E., Eriksen, C. C., Rhines, P. B., and Harcourt, R. R.: Determining vertical water velocities from Seaglider, Journal of Atmospheric and Oceanic Technology, 28, 1641 – 1656, 2011.

Frajka-Williams, E., Brearley, J. A., Nash, J. D., and Whalen, C. B.: New technological frontiers in ocean mixing, in: Ocean mixing: drivers, mechanisms and impacts, edited by Meredith, M. P. and Naveira Garabato, A. C., Elsevier Science, Amsterdam, The Netherlands, 2021.

Garau, B., Ruiz, S., Zhang, W. G., Pascual, A., Heslop, E., Kerfoot, J., and Tintoré, J.: Thermal lag correction on Slocum CTD glider data, Journal of Atmospheric and Oceanic Technology, 28, 1065 – 1071, 2011.

George, J. V., Vinayachandran, P. N., and Nayak, A. A.: Enhanced double-diffusive salt flux from the high-salinity core of Arabian Sea-origin waters to the Bay of Bengal, Journal of Physical Oceanography, 51, 505 – 518, 2021.

Howatt, T., Waterman, S., and Ross, T.: On using the finescale parameterisation and Thorpe scales to estimate turbulence from glider data, Journal of Atmospheric and Oceanic Technology, 38, 1187 – 1204, 2021.

Ijichi, T. and Hibiya, T.: Observed variations in turbulent mixing efficiency in the deep ocean, Journal of Physical Oceanography, 48, 1815 – 1830, 2018.

Lueck, R. G., Wolk, F., and Yamazaki, H.: Oceanic velocity microstructure measurements in the 20th century, Journal of Oceanography, 58, 153 – 174, 2002.

Mater, B. D., Venayagamoorthy, S. K., St Laurent, L., and Moum, J. N.: Biases in Thorpe-scale estimates of turbulence dissipation. Part 1: assessments from large-scale overturns in oceanographic data, Journal of Physical Oceanography, 45, 2497 – 2521, 2015.

Naveira Garabato, A. C., Polzin, K. L., Ferrari, R., Zika, J. D., and Forryan, A.: A microscale view of mixing and overturning across the Antarctic Circumpolar Current, Journal of Physical Oceanography, 46, 233 – 254, 2016.

Osborn, T. R.: Estimates of the local rate of vertical diffusion from dissipation measurements, Journal of Physical Oceanography, 10, 83 – 89, 1980.

Osborn, T. R. and Cox, C. S.: Oceanic fine structure, Geophysical Fluid Dynamics, 3, 321 – 345, 1972.

Ozmidov, R. V.: On the turbulent exchange in a stably stratified ocean, Atmospheric and Oceanic Physics, 8, 853 – 860, 1965.

https://doi.org/10.5194/egusphere-2022-361
Preprint. Discussion started: 31 May 2022

Palmer, M. R., Stephenson, G. R., Inall, M. E., Balfour, C., Düsterhus, A., and Green, J. A. M.: Turbulence and mixing by internal waves in the Celtic Sea determined from ocean glider microstructure measurements, Journal of Marine Systems, 144, 57 – 69, 2015.

Peterson, A. K. and Fer, I.: Dissipation measurements using temperature microstructure from an underwater glider, Methods in Oceanography, 10, 44 – 69, 2014.

Polzin, K. L., Naveira Garabato, A. C., Huussen, T. N., Sloyan, B. M., and Waterman, S.: Finescale parameterizations of turbulent dissipation, Journal of Geophysical Research: Oceans, 119, 1383 – 1419, 2014.

Radko, T. and Smith, P. D.: Equilibrium transport in double-diffusive convection, Journal of Fluid Mechanics, 690, 5 – 27, 2012.

Rainville, L., Gobat, J. L., Lee, C. M., and Shilling, G. B.: Multi-month dissipation estimates using microstructure from autonomous underwater gliders. Multi-month dissipation estimates using microstructure from autonomous underwater gliders., Oceanography, 30, 49 – 50, 2017.

Rollo, C., Heywood, K. J., and Hall, R. A.: Glider observations of thermohaline staircases in the tropical North Atlantic using an automated classifier, Geoscientific Instrumentation, Methods and Data Systems, 2022.

Ruddick, B., Anis, A., and Thompson, K.: Maximum likelihood spectral fitting: the Batchelor spectrum, Journal of Atmospheric and Oceanic Technology, 17, 1541 – 1555, 2000.

Scheifele, B., Waterman, S., Merckelbach, L., and Carpenter, J. R.: Measuring the dissipation rate of turbulence kinetic energy in strongly stratified, low-energy environments: a case study from the Arctic Ocean, Journal of Geophysical Research: Oceans, 123, 5459 – 5480, 2018.

Schmitt, R. W.: Mixing in a thermohaline staircase, in: Small-scale turbulence and mixing in the ocean: proceedings of the 19th International Liège Colloquium on ocean hydrodynamics, edited by Nihoul, J. C. J. and Jamart, B. M., pp. 435 – 452, Elsevier, Amsterdam, The Netherlands, 1988.

Schmitt, R. W., Perkins, H., Boyd, J. D., and Stalcup, M. C.: C-SALT: an investigation of the thermohaline staircase in the western tropical North Atlantic, Deep-Sea Research, 34, 1655 – 1665, 1987.

Schultze, L. K. P., Merckelbach, L. M., and Carpenter, J. R.: Turbulence and mixing in a shallow shelf sea from underwater gliders, Journal of Geophysical Research: Oceans, 122, 9029 – 9109, 2017.

Scott, R. M., Brearley, J. A., Naveira Garabato, A. C., Venables, H. J., and Meredith, M. P.: Rates and mechanisms of turbulent mixing in a coastal embayment of the West Antarctic Peninsula, Journal of Geophysical Research: Oceans, 126, e2020JC016 861, 2021.

Sheen, K. L., Brearley, J. A., Naveira Garabato, A. C., Smeed, D. A., Waterman, S., Ledwell, J. R., Meredith, M. P., St Laurent, L., Thurnherr, A. M., Toole, J. M., and Watson, A. J.: Rates and mechanisms of turbulent dissipation and mixing in the Southern Ocean: results from the Diapycnal and Isopycnal Mixing Experiment in the Southern Ocean (DIMES), Journal of Geophysical Research: Oceans, 118, 2774 – 2792, 2013.

Sommer, T., Carpenter, J. R., Schmid, M., Lueck, R. G., and A., W.: Revisiting microstructure sensor responses with implications or double-diffusive fluxes, Journal of Atmospheric and Oceanic Technology, 30, 1907 – 1923, 2013.

Stevens, B., Bony, S., Farrell, D., Ament, F., Blyth, A., Fairall, C., Karstensen, J., Quinn, P. K., et al.: EUREC4A, Earth System Science Data, 13, 4067 – 4119, 2021.

Thorpe, S. A.: Turbulence and mixing in a Scottish loch, Philosophical Transactions of the Royal Society of London, 286A, 125 – 181, 1977.

van der Boog, C. G., Dijkstra, H. A., Pietrzak, J. D., and Katsman, C. A.: Double-diffusive mixing makes small contribution to the global ocean circulation, Nature Communications Earth & Environment, 2, 46, 2021.

Whalen, C. B.: Best practices for comparing ocean turbulence measurements across spatiotemporal scales, Journal of Atmospheric and Oceanic Technology, 38, 837 – 841, 2021.

Whalen, C. B., Talley, L. D., and MacKinnon, J. A.: Spatial and temporal variability of global ocean mixing inferred from Argo profiles, Geophysical Research Letters, 39, L18 612, 2012.

Whalen, C. B., MacKinnon, J. A., Talley, L. D., and Waterhouse, A. F.: Estimating the mean diapycnal mixing using a finescale parameterisation, Journal of Physical Oceanography, 45, 1174 – 1188, 2015.